Soft Matter

COMMUNICATION

Cite this: *Soft Matter*, 2020, **16**, 4110

Received 8th February 2020,
Accepted 6th April 2020

DOI: 10.1039/d0sm00224k

rsc.li/soft-matter-journal

The tripeptide GHG as an unexpected hydrogelator triggered by imidazole deprotonation†

Morgan Hesser,[a] Lavenia Thursch,[b] Todd Lewis,[b] David DiGuiseppi,[a] Nicolas J. Alvarez *[b] and Reinhard Schweitzer-Stenner *[a]

The tripeptide glycyl-histidyl-glycine (GHG) self-assembles into long, crystalline fibrils forming a strong hydrogel ($G' \sim 50$ kPa) above a critical concentration of 40 mM upon the deprotonation of its imidazole group. Spectroscopic data reveal a mixture of helically twisted β-sheets and monomers to coexist in the gel phase.

Over the last 10 years short peptides (di- and tri-peptides) have emerged as cost-effective building blocks for supramolecular ensembles such as nanotubes and gels.[1–6] It is generally believed that the self-assembly of peptides into fibrils requires amino acid residues with aromatic side chains and end groups (*e.g.* Fmoc: fluorenylmethyloxycarbonyl). Fmoc has been shown to engage in hydrophobic interactions and cation–π interactions, both of which contribute to self-assembly.[4,7–9] However, this notion has been challenged recently by the discovery that the unblocked cationic tripeptide with the sequence GAG self-assembles into large scale fibrils, which at high concentrations form a sample spanning network.[10–12] In line with the earlier emphasized role of side chain aromaticity, DiGuiseppi *et al.* discovered that upon deprotonation of its imidazole group, GHG forms similarly large scale fibrils in water.[13] A gel network formed by GHG deprotonation is more suitable for biomedical applications than other low molecular weight peptides since its formation neither involves organic solvents nor very acidic or alkaline conditions.[14] Deprotonated imidazole groups have been shown before to induce gelation of to peptide derivatives. However, such compounds either contained additional aromatic moieties and aliphatic chains[15,16] or multiple imidazole groups.[17,18] Using Fmoc as a capping group increases aggregation of the histidine containing dipeptide L-carnosine,[19] even at pH 3 where the imidazole group of the histidine residue is protonated. In this communication, we show that under the right conditions, namely pH values favoring the deprotonated state of the imidazole, the unblocked tripeptide GHG (Fig. S1, ESI†) self-assembles into long fibrils in "haystack"-like aggregates with remarkable rheological properties despite lacking additional groups that favor gelation.

Our initial step was to create a phase diagram which illustrates how the critical concentration for the fibrilization of GHG is dependent on pH. To this end, we first dissolved the peptide in water at acidic pH (between 2 and 3) in Eppendorf cuvettes and subsequently titrated the sample to the desired pH by adding an appropriate amount of NaOH (*cf.* Material and Methods). An image of the samples produced at various pH and peptide concentrations is shown in Fig. S2 (ESI†). Thus, we obtained the phase diagram in Fig. 1, wherein filled circles denote experimental conditions probed. No visible fibril aggregates were obtained in the red region of the phase diagram after 2 weeks. The yellow area denotes a region where large fibrils became visible while the sample was inhomogeneous

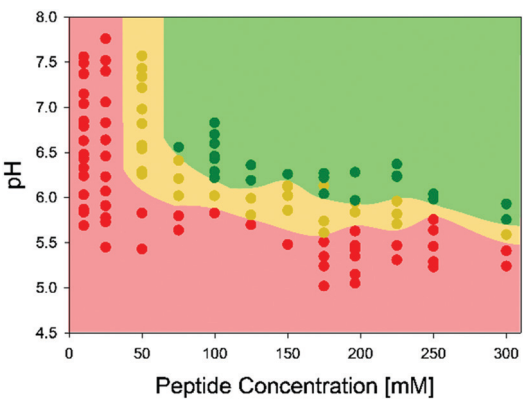

Fig. 1 Phase diagram of GHG in water with respect to peptide concentration and solution pH. Samples were characterized visually as those showing no visible large-scale peptide aggregates (red dots), those with partial aggregation (yellow dots), and nearly complete aggregation (green dots). The background has been added as a visual guide for the identification of phases.

[a] *Department of Chemistry, Drexel University, 3141 Chestnut Street, Philadelphia, PA 19104, USA. E-mail: rschweitzer-stenner@drexel.edu*

[b] *Department of Chemical and Biological Engineering, Drexel University, 3141 Chestnut Street, Philadelphia, PA 19104, USA*

† Electronic supplementary information (ESI) available. See DOI: 10.1039/d0sm00224k

and translucent. The green region represents a state with a significant number of aggregates such that the samples were opaque (Fig. S2, ESI†). Overall, the phase diagram in Fig. 1 indicates a critical concentration of *ca.* 40 mM below which we did not observe visible aggregation irrespective of the pH value. When samples in the green region were subjected to the addition of acid, the sol state of the system was recovered. Hence, the obtained phase transition is reversible.

The p*K*-value of the imidazole group of histidine in water is 6. This value can move up or down in peptides and proteins, depending on the respective environment.[20] The phase diagram in Fig. 1 suggest that self-assembly initiates just below the p*K*-value of the imidazole group. In order to provide a suitable reference point, we measured the UV-circular dichroism (UVCD) spectra of GHG as a function of pH between 2 and 11 for a peptide concentration of 10 mM, which lies below the critical concentration for visible scale self-assembly. As shown in Fig. S3 (ESI†), the UVCD spectrum is clearly pH-dependent which reflects the different degree of electronic coupling between imidazole and peptide backbone transitions in the two protonation states.[21,22] The measured spectra depict an isodichroic point within the limits of spectral noise, which indicates the expected two-state transition. Fig. S4 (ESI†) displays the dichroism value measured at 195 nm, $\Delta\varepsilon_{195}$, as a function of pH. A Henderson–Hasselbach type analysis yielded a p*K*-value of 6.48 ± 0.08. The phase diagram in Fig. 1 indicates that the critical pH decreases from *ca.* 6.4 to 5.8 upon increasing the peptide concentration from 40 to 300 mM. This observation reflects that the critical number of fibrils for large scale aggregation becomes available at lower pH.

Microscopy, rheology, and spectroscopy were all performed on a sample with 175 mM GHG within a pH close to 6.4 which lies in the green area just above the boundary between the yellow and green areas close to the mean concentration used for the well plate experiment. Fig. 2 shows a microscope image of a GHG sample at pH = 6.4 (*cf.* Material and methods). The sample spanning network can be described as overlapping various sized ''haystacks'' composed of comparatively needle-like fibrils with lengths in the sub-millimeter regime. The haystacks appear intertwined or entangled, which is expected to lead to a volume spanning network, *i.e.* hydrogel. At these conditions, the fibril network is relatively sparse, and the pore size is very large. We expect that the pore size is a strong function of GHG concentration. Note that these structures are very different than the ''sea urchin''-like structures formed by GAG in water-ethanol mixtures[12] and that they are qualitatively different from the much shorter and thinner nano-scale fibrils formed by aromatically blocked FmocFF and its derivatives.[2,6,8]

Rheological tests were conducted to determine whether a volume spanning network was formed by the haystack aggregates. The result of a frequency sweep spanning four orders of magnitude (10^{-2} to 100 rad s^{-1}) of 175 mM GHG at pH = 6.4 is shown in Fig. 3. The amplitude strain used was 0.03%. At this value we are somewhat outside the linear viscoelastic regime for the highest frequencies (see amplitude sweep in Fig. S5, ESI†) but this allows us to apply a deformation that is within machine limits. The storage modulus in the investigated frequency range is higher than the loss modulus (respectively 44 kPa and 11 kPa for ω = 1 rad s^{-1}), which indicates a viscoelastic gel. The G' value is relatively high compared to other low molecular weight gelators which is to be expected given the long, entangled fibrils observed in Fig. 2. However, G' is lower than values previously reported for GAG water/ethanol gels, which may be due to the larger pores observed throughout the network. At low frequency, the moduli get closer to each other and $\tan\delta$ increases from 0.28 to 0.68, reflecting a more viscoelastic response. We also determined the softening point of 175 mM GHG at pH = 6.4 to be 58 °C using a method previously employed for GAG in water/ethanol mixtures.[23] This value is substantially above the numbers obtained for a similar concentration of GAG in water-ethanol mixtures (200 mM) which vary between 41 and 25 °C at 74 and 50 mol% ethanol, respectively.[24]

Wide-angle X-ray scattering patterns were collected for precipitated GHG and for gels formed with 175 mM GHG at pH = 6.47 (Fig. S6, ESI†). The diffraction rings are better resolved for the precipitated peptide. We integrated the 2D-patterns over an angle of 2π and observed the scattering spectra in q-space, shown in Fig. S7 (ESI†) (*cf.* Material and methods). The common peak 1.58 $Å^{-1}$ was normalized to 1. For both precipitated peptide and self-assembled fibrils, we observe identical peak positions, though the gel exhibits lower peak intensities. This observation suggests that the fibrils in the gel

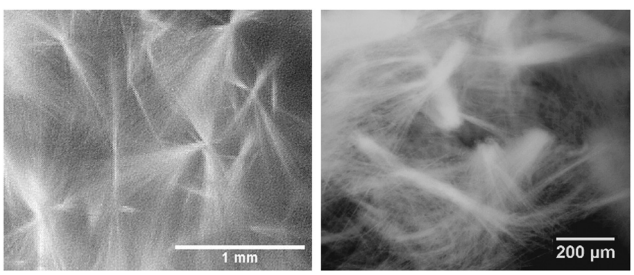

Fig. 2 Microscopic image of a GHG hydrogel formed with 175 mM peptide concentration at pH = 6.4 with the indicated resolution. The image on the left reveals the haystick character of the gel phase.

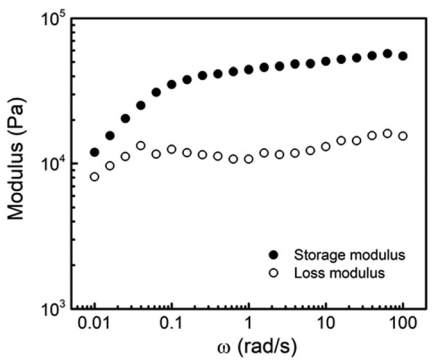

Fig. 3 Rheological frequency sweep of storage modulus (G') and loss modulus (G'') of a GHG hydrogel formed with 175 mM peptide concentration at pH = 6.4.

phase exhibit a crystalline structure similar to that in the precipitated peptide while the gel contains a more amorphous component. Peaks at 0.5–0.7 $Å^{-1}$, 1–1.1 $Å^{-1}$ and 1.4–1.6 $Å^{-1}$ regions are tentatively assigned to inter-residue, inter-strand and inter-sheet of distances of a heterogeneous ensemble of β-sheets.[25] We are currently carrying out a thorough analysis of the WAXS data of GHG and the gel phases formed by other GxG peptides. The results will be reported in a future publication.

Next, we used vibrational spectroscopy to characterize the gel phase further. Note that these measurements had to be performed in D_2O to eliminate the overlap with the HOH water bending band and vibrational mixing between peptide modes (amide I) and water.[26,27] Hence, we used DCl and NaOD to adjust the initial and final pD values. IR and VCD spectra of a 175 mM pH = 6.39 sample measured over 20 h after incubation are shown in Fig. 4. The cell was rotated approximately 120° between three measurements (the arbitrary position R1 as starting point, followed by R2, and R3) of the same sample (*cf.* the inset of Fig. 4). The VCD and IR of spectrum R2 were scaled so the IR peak intensity at 1595 cm^{-1} is identical to that of the R3 spectrum. This was done to allow for a comparison of the relative intensities of the respective VCD signals. The unscaled spectra are shown in Fig. S8 (ESI†).

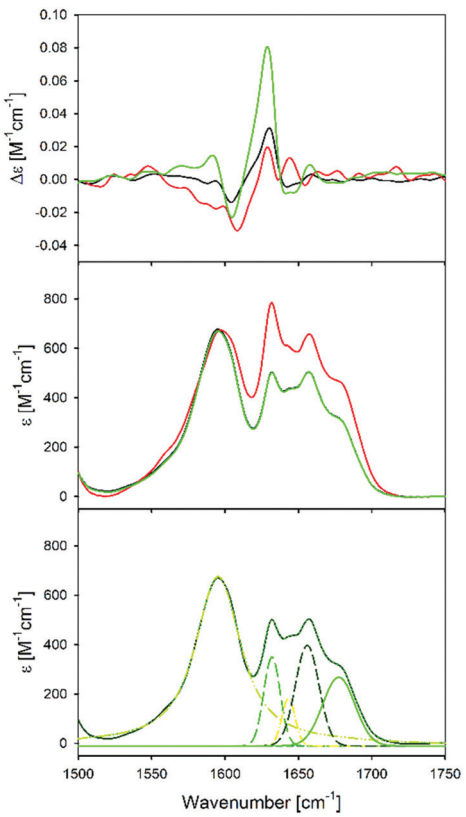

Fig. 4 VCD (top), FT-IR (middle) and spectral decomposition of FTIR (bottom) spectra of 175 mM GHG at pD = 6.39 in the region between 1500 and 1750 cm^{-1}. Sample was rotated approximately 120° between scans. The spectra are labelled as R1 (black), R2 (red), and R3 (green) in the text. Insert at top shows diagram of sample cell with the top of the cell for each rotation labelled. The spectral decomposition was performed with the R3 spectrum.

In order to properly interpret the spectra in Fig. 4 and Fig. S9 (ESI†), we revisit the amide I′ profiles in the earlier reported Raman, IR and VCD spectra of double and single protonated monomeric GHG.[13] (Fig. S7, ESI†). The doublet with peaks at 1656 and 1680 cm^{-1} is assignable to the amide I′ modes of the tripeptide. In principle, one would attribute the former to the CO stretching mode of the C-terminal peptide and the latter to the corresponding mode of the N-terminal peptide group, but excitonic coupling between the excited vibrational states mixes the wavefunctions of these states.[13] In both protonation states, the VCD signal of amide I is a weak negative couplet with an amplitude of *ca.* 0.02 M^{-1} cm^{-1}. It is diagnostic of a polyproline II/β-strand mixture of the central histidine residue.[13]

Apparently, the amide I′ profiles depicted in Fig. 4 are quite distinct from those in Fig. S7 (ESI†). The amide I′ profile of the gel phase has become more inhomogeneous. We subjected it to a spectral decomposition into sub-bands. The result is shown in the bottom panel of Fig. 4. The band at 1595 cm^{-1} is Voigtian, while the ones from 1630–1677 cm^{-1} are Gaussian. The spectral decomposition in Fig. 4 is heuristic in nature because the observed band profile is in reality underlied by a multiplet of lines assignable to transitions into delocalized vibrational states.[28] The bands at 1656 and 1677 cm^{-1} are close to the band position obtained for monomeric protonated GHG in D_2O (1656 and 1680 cm^{-1}).[29] The two bands at 1632 and 1643 cm^{-1} are in the wavenumber range of amide I′ bands assignable to β-sheet structures.[30,31] The wavenumber position depends on the number of incorporated strands (larger sheets shift the band to lower wavenumbers) and the geometry of the sheet (twisting reduces interstrand vibrational coupling and increase the amide I′ peak wavenumber).[32–34] Our spectral analysis yielded a total fractional intensity of 0.26 for the two β-sheet bands. The actual β-sheet content is likely higher because this conformation gives rise to a spectral continuum of excitonic transitions that covers the entire region between 1630 and 1690 cm^{-1}.[32,34] This continuum contributes to the 1656 and 1677 cm^{-1} band intensities obtained from our analysis.

The fibrilization on the scale shown in Fig. 2 can be expected to produce an anisotropy of the sample which could produce linear as well as circular birefringence.[35,36] Therefore, after the first measurement (R1 in Fig. 4) we rotated the sample twice by 120° and measured the IR and VCD spectra after each rotation (R2 and R3 in Fig. 4). The IR spectrum observed after the first rotation exhibits an increased β-sheet signal at 1632 cm^{-1}. In terms of rotational strength and character the amide I′ couplets in R1 and R2 are comparable with the negative couplet of the peptide monomer (Fig. S9, ESI†), but the positions of the negative and positive maxima now lie at the COO^- antisymmetric stretching band and the 1632 cm^{-1} sub-band of the amide I′ profile, respectively. The corresponding VCD signal is on the same order of magnitude as that observed for the amide I′ region of monomeric GHG.[29] The second rotation returned the IR spectrum to the same relative magnitudes. The VCD signal increased significantly. These observations suggest

that the orientation of fibrils in the sample is somewhat anisotropic which causes some birefringence. The rather high wavenumber positions and the negligible rotational strength of the 1643 cm^{-1} band are indicative of untwisted β-sheet type oligomers.[32] The VCD associated with the 1595 and 1632 cm^{-1} band is clearly pronounced but less intense than observed for GAG fibrils.[10–12] Generally, ideal β-sheets are nearly planar and give rise to very weak VCD signals.[34] A strong VCD signal like the one associated with the 1632 cm^{-1} band suggests long helically twisted β-sheet tapes integrated in peptide fibrils. Such supramolecular structures generally give rise to either a negative or positive couplet in the region of highest amide I intensity.[11,12,37,38] Here, the negative maximum is shifted to the COO^- asymmetric stretching band region. The only plausible explanation for this observation is excitonic coupling between COO^- as and amide I′ vibrations in adjacent strands where the C-terminal substitutes for the C═O group in interstrand excitonic coupling. The comparatively large wavenumber difference between these two bands reduces the mixing of wavefunctions in excitonic states compared with the interstrand coupling between amide I′ modes with identical or similar intrinsic wavenumber positions. This explains why the observed couplet is less intense than that of GAG fibrils. Furthermore, we have to take into account that β-sheets account only for 26% of the peptides. Hence, the real VCD signal would increase by a factor of four if all peptides were incorporated in fibrils.

Taken together our results suggest that deprotonated GHG forms a strong hydrogel in water. The sample spanning network is formed by large crystalline fibrils composed of β-sheet tapes. The pH at which fibrilization occurs varies with peptide concentration. Below 40 mM, no visible aggregation occurs irrespective of pH. In the region close to the boundary separating the gel phase from a less viscous phase of partially aggregated peptides (Fig. 1), amorphous aggregates and β-sheet based helical twisted fibrils coexist. The degree of fibril crosslinking is sufficient to form a rather strong gel. Future investigations will focus on the peptide concentration and pH dependence of the gel phase characteristics.

Conflicts of interest

There are no conflicts to declare.

Acknowledgements

Research reported in this paper was supported by a grant from the National Science Foundation to R. S. S. and N. J. A. (DMR-170770) and an REU-supplement for the support of M. H. (DMR-1915781). M. H. was further supported by a grant from the Steinbright Career Development Center of Drexel University.

Notes and references

1 E. Gazit, *Prion*, 2007, **1**, 32–35.
2 L. Adler-Abramovich and E. Gazit, *Chem. Soc. Rev.*, 2014, **43**, 6881–6893.
3 R. V. Ulijn, N. Bibi, V. Jayawarna, P. D. Thornton, S. J. Todd, R. J. Mart, A. M. Smith and J. E. Gough, *Mater. Today*, 2007, **10**, 40–48.
4 P. W. J. M. Frederix, G. G. Scott, Y. M. Abul-Haija, D. Kalafatovic, C. G. Pappas, N. Javid, N. T. Hunt, R. V. Ulijn and T. Tuttle, *Nat. Chem.*, 2015, **7**, 30–37.
5 I. W. Hamley, *Angew. Chem., Int. Ed.*, 2007, **46**, 8128–8147.
6 E. R. Draper and D. J. Adams, *Chem. Soc. Rev.*, 2018, **47**, 3395–3405.
7 P. W. J. M. Frederix, R. V. Ulijn, N. T. Hunt and T. Tuttle, *J. Phys. Chem. Lett.*, 2011, **2**, 2380–2384.
8 A. Mahler, M. Reches, M. Rechtier, S. Cohen and E. Gazit, *Adv. Mater.*, 2006, **18**, 1365–1370.
9 G. Cheng, V. Castelletto, C. M. Moulton, G. E. Newby and I. W. Hamley, *Langmuir*, 2010, **26**, 4990–4998.
10 B. Milorey, S. Farrell, S. E. Toal and R. Schweitzer-Stenner, *Chem. Commun.*, 2015, **51**, 16498–16501, DOI: 10.1039/c5cc06097d.
11 S. Farrell, D. DiGuiseppi, N. Alvarez and R. Schweitzer-Stenner, *Soft Matter*, 2016, **12**, 6096–6110.
12 D. DiGuiseppi, L. Thursch, N. J. Alvarez and R. Schweitzer-Stenner, *Soft Matter*, 2019, **15**, 3418–3431.
13 D. DiGuiseppi and R. Schweitzer-Stenner, *J. Raman Spectrosc.*, 2016, **47**, 1063–1072, DOI: 10.1002/jrs.4885.
14 V. Jayawarna, M. Ali, T. A. Jowitt, A. F. Miller, A. Saiani, J. E. Gough and R. V. Ulijn, *Adv. Mater.*, 2006, **18**, 611–614.
15 R. Otter, C. M. Berac, S. Seiffert and P. Besenius, *Eur. Polym. J.*, 2019, **110**, 90–96.
16 K. J. C. Van Bommel, C. Van Der Pol, I. Muizebelt, A. Friggeri, A. Heeres, A. Meetsma, B. L. Feringa and J. Van Esch, *Angew. Chem., Int. Ed.*, 2004, **43**, 1663–1667.
17 T. J. Moyer, J. A. Finbloom, F. Chen, D. J. Toft, V. L. Cryns and S. I. Stupp, *J. Am. Chem. Soc.*, 2014, **136**, 14746–14752.
18 B. F. Lin, K. A. Megley, N. Viswanathan, D. V. Krogstad, L. B. Drews, M. J. Kade, Y. Qian and M. V. Tirrell, *J. Mater. Chem.*, 2012, **22**, 19447–19454.
19 V. Castelletto, G. Cheng, B. W. Greenland, I. W. Hamley and P. J. F. Harris, *Langmuir*, 2011, **27**, 2980–2988.
20 R. L. Thurlkill, G. R. Grimsley, J. M. Scholtz and C. N. Pace, *Protein Sci.*, 2006, **15**, 1214–1218.
21 A. Chakrabartty, T. Kortemme, S. Padmanabhan and R. Baldwin, *Biochemistry*, 1993, **32**, 5560–5565.
22 S. Bhattacharjee, G. Tóth, S. Lovas and J. D. Hirst, *J. Phys. Chem. B*, 2003, **107**, 8682–8688.
23 L. Thursch, D. DiGuiseppi, T. Lewis, R. Schweitzer-Stenner and N. J. Alvarez, *J. Colloid Interface Sci.*, 2020, **564**, 499–509.
24 L. Thursch, D. DiGuiseppi, N. Alvarez and R. Schweitzer-Stenner, *J. Colloid Interface Sci.*, 2020, **564**, 499–599.
25 L. Kreplak, J. Doucet, P. Dumas and F. Briki, *Biophys. J.*, 2004, **87**, 640–647.
26 G. Sieler and R. Schweitzer-Stenner, *J. Am. Chem. Soc.*, 1997, **119**, 1720–1726.
27 N. V. Ilawe, A. E. Raeber, R. Schweitzer-Stenner, S. E. Toal and B. M. Wong, *Phys. Chem. Chem. Phys.*, 2018, **20**, 18158–18168, DOI: 10.1039/c5cp03646a.
28 A. Kumar, R. Schweitzer-Stenner and B. M. Wong, *Chem. Commun.*, 2019, **55**, 5701–5704.

29 D. DiGuiseppi and R. Schweitzer-Stenner, *J. Raman Spectrosc.*, 2016, **47**, 1063–1072.
30 S. Krimm and J. Bandekar, *Adv. Protein Chem.*, 1986, **38**, 181–364.
31 A. Barth, *Prog. Biophys. Mol. Biol.*, 2000, **74**, 141–173.
32 R. Schweitzer-Stenner, *J. Phys. Chem. B*, 2012, **116**, 4141–4153.
33 C. Lee and M. Cho, *J. Phys. Chem. B*, 2004, **108**, 20397–20407.
34 P. Bour and T. A. Keiderling, *J. Mol. Struct.*, 2004, **675**, 95–105.
35 T. Buffeteau, F. Lagugné-Labarthet and C. Sourisseau, *Appl. Spectrosc.*, 2005, **59**, 732–745.
36 M. Wolffs, S. J. George, Ž. Tomović, S. C. J. Meskers, A. P. H. J. Schenning and E. W. Meijer, *Angew. Chem., Int. Ed.*, 2007, **46**, 8203–8205.
37 T. J. Measey and R. Schweitzer-Stenner, *J. Am. Chem. Soc.*, 2011, **133**, 1066–1076.
38 S. Ma, X. Cao, M. Mak, A. Sadik, C. Walkner, T. B. Freedman, I. K. Lednev, R. K. Dukor and L. A. Nafie, *J. Am. Chem. Soc.*, 2007, **129**, 12364–12365.

